scientific reports

Check for updates

OPEN

Aducanumab delivery via focused ultrasound-induced transient blood–brain barrier opening in vivo

Jaeyeong Jeong[1,2,4], Mun Han[2,4], Soyeon Jeon[2], Yejin Kim[3], Hyo Jin Choi[2], Woohyuk Choi[2], Kihyun Kwon[2], Jong-ryul Choi[2]✉ & Eun-Hee Lee[2]✉

Focused ultrasound (FUS) with magnetic resonance imaging (MRI) guidance (MRgFUS) has emerged as a promising technique for enhancing drug delivery to the brain. Through the controlled oscillation of gas-encased microbubbles, FUS temporarily modulates the integrity of tight junctions, inducing localized blood-brain barrier disruption (BBBD) and allowing targeted drug passage. Aducanumab (ADU) has demonstrated efficacy in reducing amyloid pathology, yet its clinical application remains limited by the restrictive nature of the blood-brain barrier (BBB). This in vivo study aimed to evaluate the efficiency of ADU delivery facilitated by FUS-induced BBBD in the normal Institute of Cancer Research (ICR) mouse brain under two pressure conditions: 0.25 and 0.42 MPa. Following FUS sonication with MRI guidance, ADU concentrations in brain tissues and serum were measured via enzyme-linked immunosorbent assay (ELISA) at multiple time points. Histological analysis at 24 h post-FUS-BBBD was performed to assess ADU distribution, and tissue integrity was evaluated through hematoxylin and eosin (H&E) and Nissl staining to detect potential damage in the target regions. The results demonstrated that MRgFUS significantly increased ADU concentrations within the target areas without inducing substantial tissue damage. ADU delivery efficiency was directly correlated with the degree of BBBD, exhibiting a 7-fold increase at 0.25 MPa and a 60-fold increase at 0.42 MPa compared to sham controls, with distinct kinetic profiles observed for each condition. These findings highlight the potential of FUS-BBBD as a therapeutic strategy to enhance ADU delivery to the brain, reduce required infusion doses, and mitigate side effects associated with high-dose administration.

Keywords Blood–brain barrier, Drug delivery to a brain, Focused ultrasound, Aducanumab, Alzheimer's disease

With increasing life expectancy, a growing number of individuals worldwide are developing central nervous system (CNS) disorders, including neurodegenerative. Despite significant progress in brain disease therapeutics, clinical trials continue to face challenges related to drug efficacy and limited brain penetration[1,2]. The blood-brain barrier (BBB) is a highly selective, semi-permeable structure formed by brain endothelial cells, astrocytic end-feet, and pericytes. It plays a crucial role in maintaining brain homeostasis and neuronal function[3]. Tight junctions between endothelial cells prevent the uncontrolled passage of molecules between the bloodstream and brain tissue, allowing only small (< 400 Da) lipophilic molecules to pass through via passive lipid diffusion[4–6]. Although this function is protective, it presents a significant barrier to the delivery of therapeutics into the brain. This limitation reduces the efficacy of many CNS drugs and has contributed to the failure of several treatments for brain disorders[2,7].

Focused ultrasound (FUS)-induced BBB disruption (FUS-BBBD) has emerged as a promising strategy to enhance drug delivery to the brain, including for neurodegenerative disorders such as Alzheimer's disease (AD). This technique is noninvasive, temporally controlled, repeatable, and highly localized, making it an attractive approach for CNS drug delivery[2,8]. Unlike conventional drug delivery methods that are restricted by molecular size and lipophilicity[6], FUS-BBBD facilitates the transient transport of a wide range of therapeutics, from small molecules and antibodies to nanoparticles and even cell-based therapies[9]. By inducing the oscillation of intravenously administered microbubbles, FUS modulates tight junctions and temporarily increases BBB

[1]Department of Molecular and Cellular Biology, Baylor College of Medicine, Houston, TX 77030, USA. [2]Medical Device Development Center, Daegu-Gyeongbuk Medical Innovation Foundation (K- MEDIhub), Daegu, South Korea. [3]Preclinical Research Center, Daegu-Gyeongbuk Medical Innovation Foundation (K-MEDIhub), Daegu, South Korea. [4]Jaeyeong Jeongand Mun Han have contributed equally to this work. ✉email: jongryul32@kmedihub.re.kr; ehlee@kmedihub.re.kr

permeability, facilitating the controlled and region-specific penetration of therapeutic agents into the brain parenchyma[10].

Extensive preclinical research has demonstrated that various ultrasound parameters, including pressure amplitude, pulse duration, burst repetition frequency, and microbubble dose, play crucial roles in determining the extent and duration of BBB opening[11–13]. Among these parameters, acoustic pressure plays a critical role in modulating BBB permeability and drug distribution efficiency. Higher pressures generally lead to greater BBB disruption but may also increase the risk of vascular damage[14,15]. MRI-guided FUS (MRgFUS) further enhances the precision and safety of this approach by enabling real-time monitoring of BBB opening, optimizing therapeutic outcomes while minimizing potential adverse effects[16]. As a result, FUS-BBBD is increasingly being investigated for its potential to improve CNS drug delivery and expand treatment options for neurological disorders.

Aducanumab (ADU; Aduhelm, Biogen, Neurimmune) is a human IgG1 monoclonal antibody designed to bind to the N-terminus of amyloid-beta (Aβ) (residues 3–7), selectively targeting Aβ aggregates, including insoluble fibrils and soluble oligomers, while exhibiting low affinity for monomeric Aβ[17]. By promoting the phagocytosis of Aβ and protecting neural tissues from toxic Aβ oligomers, ADU has been shown to slow the progression of Alzheimer's disease (AD)[18]. In June 2021, the U.S. Food and Drug Administration approved for ADU in the treatment of mild cognitive impairment (MCI) and early-stage AD under the accelerated approval pathway[19–21]. However, post-approval trials ('221AD301 Phase 3 Study of Aducanumab in Early Alzheimer's Disease [NCT02477800]' and '221AD302 Phase 3 Study of Aducanumab in Early Alzheimer's Disease [NCT02484547]') revealed that while high-dose ADU (10 mg/kg) was effective in early-stage AD【NCT02484547】, its clinical benefits remain debated. Despite its therapeutic potential, high doses have been linked to amyloid-related imaging abnormalities (ARIA), including edema (ARIA-E) and microhemorrhages (ARIA-H)[22,23]. These challenges underscore the need for optimized drug delivery strategies that enhance brain penetration while minimizing adverse effects, particularly at lower doses. Focused ultrasound (FUS) with microbubbles enables transient, localized BBB disruption (FUS-BBBD), providing a promising approach to enhance ADU delivery to the brain.

Previous studies have demonstrated the efficacy of FUS-BBBD in improving ADU penetration. Kong et al. reported that FUS combined with low-dose ADU (3 mg/kg) increased brain ADU concentration 8.1-fold, leading to a significant reduction in Aβ plaques and improved cognitive function in 5×FAD mice, without exacerbating neuroinflammation or microhemorrhages[24]. Similarly, Leinenga et al. found that FUS-assisted ADU delivery enhanced Aβ clearance in both the hippocampus and cortex of APP23 mice, with a fivefold increase in brain ADU levels and superior spatial memory improvement compared to ADU alone[25]. However, these studies utilized a single ultrasound pressure level, limiting the ability to assess how varying acoustic pressures influence BBB permeability and ADU delivery. Furthermore, there remains a lack of comprehensive pharmacokinetic analyses of ADU following FUS-BBBD, particularly in non-diseased models.

In this study, we investigated the potential of FUS-BBBD to enhance the delivery of ADU to the brain. We tested two different FUS parameters (0.25 MPa and 0.42 MPa) to determine their effects on ADU delivery and to examine the correlation between the degree of BBB disruption and ADU concentration in brain parenchyma in vivo. ADU was administered following FUS-BBBD under MRI guidance, and ADU kinetics and distribution were analyzed at various time points using enzyme-linked immunosorbent assay (ELISA) and immunohistochemistry. Hematoxylin and eosin (H&E) and Nissl staining were performed to assess potential tissue damage in the FUS-targeted brain regions. Our results demonstrate that FUS-BBBD significantly increases ADU delivery, with the amount of drug delivered correlating with the extent of BBB disruption. These findings suggest that FUS-BBBD may be a powerful therapeutic approach to enhance drug delivery to the brain.

Materials and methods

Animals

All animal care and experiments were performed in accordance with the guidelines of the Institutional Animal Care and Use Committee of Daegu-Gyeongbuk Medical Innovation Foundation (IACUC approval number: KMEDI-22012601-00). ICR (Institute of Cancer Research) mice (8-weeks-old, 32 ± 2.6 g), which were purchased by Koatech (Pyeongtaek, Republic of Korea), were housed in temperature- (20–25℃) and humidity-controlled conditions under a 12-h light/dark cycle. Throughout the housing and experiments, all animals had free access to food and water. Animals that were not included in the experimental groups or were euthanized based on weight criteria underwent CO_2 euthanasia in accordance with ethical guidelines. All experiments were conducted with the minimum number of animals necessary to produce significant scientific data.

Study design

ICR mice were randomly assigned to one of the following three groups: two sonication groups determined by magnetic resonance (MR) signal analysis and a sham control group. The two sonication groups were designed with 0.25 or 0.42 MPa of acoustic power[26]. Four BBBD sonication points were used for ELISA and immunohistochemistry assays. MRI images were cropped before [T2-weighted (T2W)] and after FUS-BBBD [T1-weighted (T1W)], followed by ADU administration and animal sacrifice at each time point (Fig. 1C).

One hundred four male ICR mice were used in this study, with their distribution across treatment groups summarized in the Table 1. The first ten ICR mice were used in a pilot study to define FUS parameters setup for BBBD conditions, and the dynamic contrast-enhanced MRI (DCE-MRI) image optimization, and ELISA and immunohistochemical staining (IHC) setup tests. Seventy-two ICR mice were used in the ELISA. Four ICR mice were assigned to each time point of 1, 8, 24, 72, 168, and 336 h in three groups (two sonication groups and sham control group), respectively. For the IHC, sixteen ICR mice were used, four mice each in the untreated control

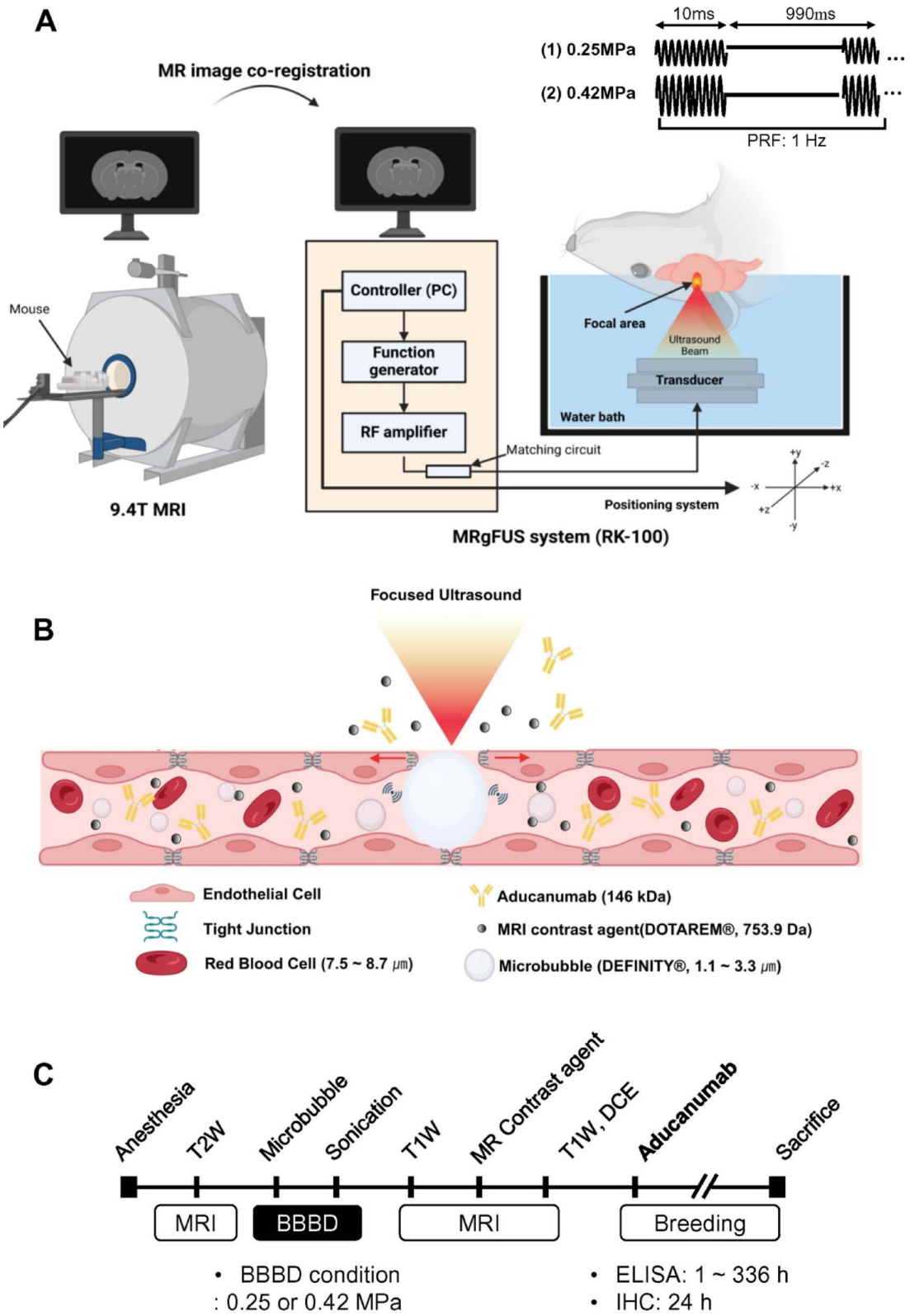

Fig. 1. (**A**) A schematic diagram of the focused ultrasound with magnetic resonance imaging guidance (MRgFUS) system. (**B**) A conceptual diagram of focused ultrasound-induced blood-brain barrier (BBB) opening. (**C**) An experimental design of procedures for in vivo study of Aducanumab delivery via focused ultrasound-induced BBB opening.

Experimental group	Pilot study	ELISA	Histology (IHC, H&E, Nissl)
Normal	10	-	4
Sham		24	4
0.25 MPa		28	4
0.42 MPa		26	4

Table 1. Summary of animal numbers.

group and the Sham group that received only no FUS sonication, and for mice each in the two sonication groups, respectively. Four ICR mice were used for H&E and Nissl staining to assess damage inflicted on the rat brain.

BBBD system

As described previously[27–29], the MRI-guided focused ultrasound (MRgFUS; RK-100, FUS Instruments, Toronto, Canada) system was used to perform FUS-induced BBB disruption. A schematic representation of this system is shown in Fig. 1A. This system comprises a single-element therapeutic FUS transducer (diameter: 75 mm, radius: 60 mm, center frequency: 1.2 MHz) and a computer-controlled 3D positioning system. Prior to sonication, the FUS pressure distribution in the focal region was measured in a free-water field using an acoustic intensity measurement system (AIMS III; ONDA Corporation, Sunnyvale, CA, USA) and a hydrophone (HGL-400; ONDA Corporation)[28]. Briefly, the transducer was submerged in a tank filled with degassed water and controlled using a three-dimensional positioning system. The ultrasound focal region was characterized using hydrophone measurements at both 0.25 MPa and 0.42 MPa. The peak acoustic pressure and mechanical index (MI) distributions were mapped to confirm the spatial characteristics of the ultrasound beam, as shown in **Supplementary Fig. 1**. The full width at half maximum (FWHM) of the ultrasound beam was measured to be approximately 2 mm in the lateral direction and 13 mm in the axial direction for 0.25 MPa and 0.42 MPa. The animal was placed on an MRI-compatible bed in the supine position, with its upper head partially submerged in a water bath. Guided by images obtained from MRI, the transducer was moved to a specific region of the mouse brain for sonication. To ensure accurate target localization, T2-weighted MRI images were acquired using the 9.4-T preclinical MRI system (Biospec 94/20 USR; Bruker, Ettlingen, Germany). The target coordinates were identified based on anatomical landmarks and manually registered to the RK-100 ultrasound system. The MRI images were then transferred from the Bruker computer to the RK-100 system, ensuring precise alignment between the MRI-defined target region and the ultrasound focal spot. The detailed mechanism of FUS-induced BBB opening is presented in Fig. 1B.

BBBD experiments

As described previously[26–29], mice weighing 33–35 g were anesthetized by administering a mixture of Zoletil (Tiletamine + Zolazepam, 25 mg/kg; Virbac, Carros, France) and Rompun (Xylazine, 4.6 mg/kg; Bayer, Leverkusen, Germany) into a hind leg muscle of the mice. Based on 30 g of mice, a 30 µL volume of the anaesthetic mixture was applied. And mice were constantly monitored throughout the entire experimental procedure. After shaving their hair, animals were placed on an MR-compatible animal bed (Fig. 1A). Based on the MRI images, the transducer was moved to the target region, and microbubbles (0.02 mL/kg, diluted in a 1:50 ratio with normal saline. Microbubble infusion was performed using an automated syringe pump (Harvard Apparatus, Holliston, MA, USA) through the tail vein. A diluted microbubble solution (Definity; Lantheus Medical Imaging, North Billerica, MA, USA) was administered at a rate of 90 s, with a total volume of 0.02 mL/kg. Sonication was initiated 10 s after the injection of the microbubble solution and continued for 90 s during infusion[30]. Then, one of the two acoustic pressure conditions, i.e., 0.25 MPa or 0.42 MPa[26], was applied to induce BBB disruption in the target region containing the cortex, hippocampus (HP), and thalamus (TH). The hippocampus-including thalamus was selected as the target region due to its relevance in AD and reproducible BBB opening. The set options of FUS energy were 10 ms of tone bursts and 1 Hz of pulse repetition frequency for 120 s. To confirm the degree of BBBD after sonication, T1W MR images were obtained with a gadolinium-based contrast agent (0.2 mM/kg; Dotarem; Guerbet, Villepinte, France). After FUS-induced BBB disruption, ADU (aducanumab biosimilar; 3 mg/kg, diluted with phosphate-buffered saline (PBS; Proteogenix, Schiltigheim, France) was injected through the tail vein. For ADU quantification, blood samples were collected from the inferior vena cava (IVC) at each time point, followed by cardiac perfusion with 0.9% saline, after which the brain was extracted. For tissue staining, mice underwent transcardial perfusion with 0.9% saline, followed by fixation with 4% formaldehyde.

MRI and dynamic contrast-enhanced (DCE)-MRI

Imaging was performed using a 9.4-T preclinical MRI system (Biospec 94/20 USR; Bruker, Ettlingen, Germany). Before FUS sonication, T2W images were used to locate target brain regions. To assess BBB opening, pre-contrast T1W images were acquired before contrast administration, followed by post-contrast T1W imaging after FUS sonication to evaluate the degree of BBB disruption. The MRI parameters were used for two-dimensional rapid acquisition with refocused echoes in this study; T1W images: field of view = 30 mm x 30 mm, matrix size = 256 × 256, axial slices/ thickness = 26/ 1.0 mm, coronal slices/ thickness = 10/ 1.5 mm, slice gap = 0, repetition time (TR) = 1,500 ms, echo time (TE) = 6.5 ms, and number of averages = 3; T2W images: field of view = 30 mm x 30 mm, matrix size = 256 × 256, axial slices/ thickness = 26/ 1.0 mm, coronal slices/ thickness = 10/ 1.5 mm, slice

gap = 0, TR = 2,500 ms, TE = 33 ms, number of averages = 2. The animals' body temperatures were maintained at approximately 37℃ during the MRI scan using a warm water blanket.

To evaluate the degree of BBBD in T1W images, the contrast-enhanced signal intensity was normalized to the background noise signal intensity. For signal intensity analysis, regions of interest (ROIs) were consistently measured using a 0.75 mm^2 rectangular ROI. This standardized ROI size ensured uniformity across all analyses. The signal intensities of the contrast agent in the ROI were analyzed, and changes in the MR signal intensity between the FUS-sonicated and contralateral regions were described in terms of percentage.

To evaluate the dynamics of contrast agents in the brain, we performed DCE-MRI[31–33]. Pre-contrast T1-weighted (T1W) images were acquired before the scan. During dynamic imaging, a contrast agent was administered, and T1W images were continuously acquired to monitor signal intensity changes over time. DCE-MRI was performed using a two-dimensional Fast Low Angle Shot (FLASH) sequence with the following parameters: field of view = 35 mm × 35 mm, matrix size = 128 × 128, coronal slices/thickness = 5/1.0 mm, slice gap = 0, repetition time (TR) = 24.2 ms, echo time (TE) = 1.4 ms, number of averages = 3, temporal resolution = 9.3 s, repetitions = 70, and total scan time = 10 min 51 s. The contrast agent traverses the vascular endothelium of the BBB and enters the extravascular and extracellular spaces (EES). By analyzing the T1W MR sequences, DCE-MRI was used to measure the signal intensity changes of the contrast agent in rapid succession. We used the DCE@urLAB software[32] to calculate the K_{trans} value and the volume of the transfer constant between the plasma and EES. We adopted the Tofts model, a bi-exponential model for the concentration of contrast agents in the blood plasma, for pharmacokinetic analysis of T1W DCE-MRI[34].

ELISA

Animals were deeply anesthetized with an overdose of a mixture of Zoletil and Rumpun at 1, 8, 24, 72, 168, and 336 h after FUS-induced BBBD. Approximately 1 mL of blood was collected from each animal into a heparin-coated tube. The animals were then perfused transcardially with 0.9% normal saline, and the brain region covering both the HP and CP was rapidly removed. ELISA was performed according to the user protocol for the Human IgG ELISA kit (Abcam, Cambridge, UK). Briefly, brain tissues were homogenized with cell extraction buffer, centrifuged at 18,000 × g for 20 min, and the supernatant was collected for further analysis. Plasma was isolated from mouse blood samples by centrifugation at 3,000 rpm for 10 min, yielding approximately 500 µL of plasma per sample. Then, 150 µL of brain or plasma samples were incubated with 150 µL of an antibody cocktail, a mixture of human IgG capture antibody and detector antibody, in a SimpleStep Pre-coated 96-well microplate at room temperature on a shaker for 1 h. The microplate was then washed with wash buffer PT, incubated with TMB development solution for 5 min, and mixed with stop solution, and the optical density of each well was recorded at 450 nm. Measurements of the standards and samples were performed in triplicate on the same plate, and the recorded values of the samples were calibrated based on the standard curve measured in the same trial.

Immunohistochemistry, hematoxylin & Eosin (H&E) staining, and Nissl staining

Animals were deeply anesthetized with an overdose of a mixture of Zoletil and Rumpun and perfused transcardially with 0.9% normal saline, followed by 4% paraformaldehyde in 0.1 M phosphate buffer (pH 7.4; #P2007-1; Biosesang, Sengnam-si, Gyeonggi-do, Korea) after 24 h of FUS-induced BBBD. After post-fixing and incubation with 30% sucrose solution, brains were coronally cut at 30-µm-thick using cryostat (CM1850; Leica Biosystems, Nussloch, Germany). Serial coronal sections were processed for IHC, H&E staining, and Nissl staining[27,28].

For IHC, the brain sections were rinsed with PBS and permeabilized with 0.2% Triton X-100 (#X100; Sigma-Aldrich, St. Louis, MO, USA) in PBS containing 1% bovine serum albumin (BSA; #422381B; VWR Life Science, Cleveland, OH, USA) for 30 min. Sections were then blocked with PBS containing 2% normal goat serum (#93951-72; Vector Laboratories, Burlingame, CA, USA) and 3% BSA for 1 h and incubated with a fluorescence-conjugated secondary antibody (goat anti-human Alexa Fluor 555; #A214433; Invitrogen, Waltham, MA, USA) at room temperature on a shaker for 1 h. After rinsing with PBS, the labeled sections were covered with Vectashield mounting medium (#H-1200-10; Vector Laboratories) for fluorescence staining with DAPI (4′,6-diamidino-2-phenylindole). For H&E staining, the brain sections were mounted on adhesive microscope slides and dried. Subsequently, the sections were hydrated with xylene and ethanol for ready penetration of the aqueous reagents into the cells and tissues. The sections were then stained with hematoxylin (#H3502; Vector Laboratories) for 5 min and differentiated with mild acid to remove nonspecific background staining. Next, sections were applied by bluing reagent, stained with Eosin Y solution (#H3502; Vector Laboratories) for 2 min, dehydrated with ethanol and xylene, and covered by a coverslip. For Nissl staining, the mounted sections were defatted with xylene and ethanol, stained with 0.5% cresyl violet acetate solution (#C5042; Sigma-Aldrich), differentiated with ethanol, dehydrated with ethanol and xylene, and covered with a coverslip. All histopathological images, including H&E and Nissl-stained sections, were captured at 10x magnification, while all immunofluorescence images were captured at 20x magnification using a digital slide scanner (Axio Scan.Z1; Carl Zeiss, Oberkochen, Germany).

Immunostaining image analysis

Immunostaining images obtained from the slide scanner were analyzed using the ImageJ™ software[35] (National Institutes of Health, Bethesda, MD, USA), and intensity value of each pixel in the immunostaining images were quantitatively analyzed. To be specific, ImageJ™ was used to quantify the chromogenic signal intensities of the immunostaining images. To measure the ADU distribution, images were transformed to 8-bit grayscale, adjusted above the threshold to rule out nonspecific background signals, and intensity values of pixels were quantified from four tissues of each brain sample. Quantified values of the samples were normalized to those of the sham control.

Statistical analysis

Statistical analyses were performed using GraphPad Prism 8 software (Dotmatics, Bishop Stortford, UK). Results are expressed as mean ± standard error of the mean (SEM) or mean ± standard deviation (SD), as indicated. For comparison of multiple groups, p value was assessed by one-way or two-way analysis of variance (ANOVA) with Tukey's multiple comparison test. Significance was set at $p < 0.05$.

Results

BBB disruption via FUS-induced BBBD in vivo

To evaluate the effectiveness of FUS-mediated BBB disruption, we applied FUS sonication to induce BBBD in the mouse brain using two different acoustic pressure conditions: 0.25 MPa and 0.42 MPa. The extent of BBBD was confirmed by analyzing the signal intensity of a contrast agent in T1W MRI images of the FUS-targeted region, acquired 5 min post-sonication (Fig. 1C). Representative MR images of both conditions are displayed for the sham control (Figs. 2A-C). Signal intensity within the region of interest (ROI) increased significantly by 55.2 ± 3.8% at 0.25 MPa ($p < 0.0001$) and 97.5 ± 4.4% at 0.42 MPa ($p < 0.0001$) compared to the contralateral non-sonicated regions (Fig. 2D). Additionally, the permeability dynamics of FUS-induced BBBD were assessed over

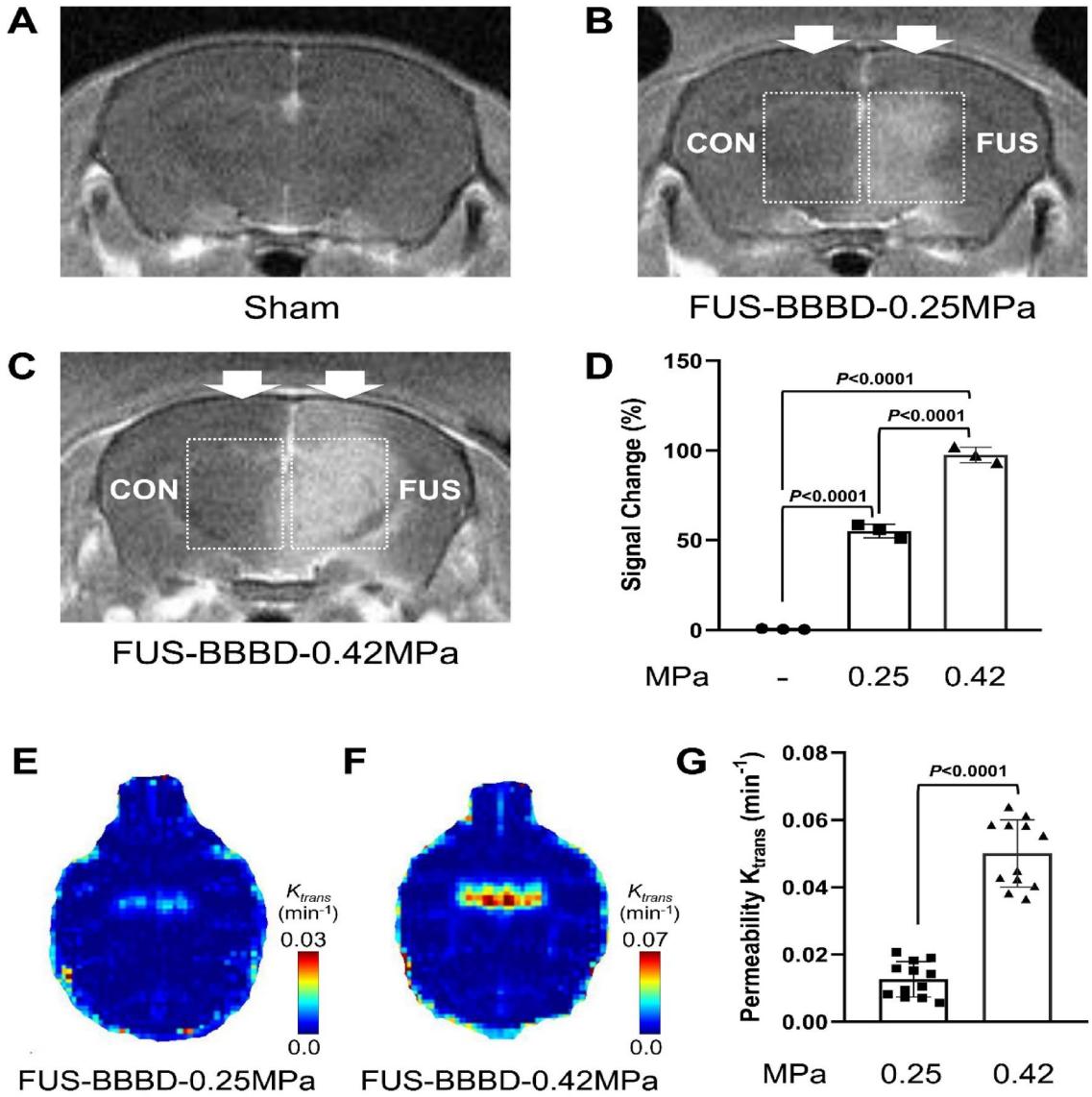

Fig. 2. Postoperative contrast agent-enhanced magnetic resonance imaging and permeability maps after the FUS-BBBD. (**A**-**C**) Contrast T1W magnetic resonance images of ICR mouse brains acquired 5 min after FUS-BBBD with (A) no acoustic pressure (sham), (**B**) 0.25 MPa, and (**C**) 0.42 MPa. (**D**) Quantitative estimation of signal intensity changes of the region-of-interest in the contrast-enhanced T1W magnetic resonance images after FUS-BBBD. (**E**-**F**) Permeability maps calculated by contrast-enhanced magnetic resonance images measured 5 min after FUS-BBBD with (**E**) 0.25 MPa and (**F**) 0.42 MPa. (**G**) Quantitative estimation of permeability (K_{trans}) from the calculated permeability maps.

a 5-minute period following sonication using DCE-MRI (Figs. 2E, F). In the 0.25 MPa group, the K_{trans} value was 0.012 ± 0.005 min^{-1}, while in the 0.42 MPa group, K_{trans} reached 0.05 ± 0.01 min^{-1} (Fig. 2G). The K_{trans} value in the 0.42 MPa group was approximately four times higher than that in the 0.25 MPa group ($p < 0.0001$). These results are consistent with our previous findings, showing a similar trend[26].

Enhanced drug delivery via FUS-induced BBBD in vivo

Previous studies, including our own, have shown that FUS-BBBD significantly enhances the delivery of therapeutic agents to the brain by transiently disrupting the BBB[1,24,25,29]. To assess whether FUS-BBBD facilitates increased drug delivery, we administered a single intravenous dose of Aducanumab(ADU, 3 mg/kg) following FUS-BBBD. ADU concentrations in both brain tissue and plasma were measured at multiple time points (1, 8, 24, 72, 168, and 336 h post-injection). The maximum concentration (C_{max}) of ADU in the brain, defined as the highest observed concentration across all time points, was 45.1 ± 19.2 ng/g at 168 h in the sham control group, 199.9 ± 57.0 ng/g at 8 h in the 0.25 MPa group, and 1,217 ± 333.3 ng/g at 24 h in the 0.42 MPa group. Notably, the C_{max} in the 0.42 MPa group was significantly higher than that in both the Sham and 0.25 MPa groups ($P < 0.0001$). At 168 h, ADU concentrations were 44.2 ± 13.7 ng/g in the 0.25 MPa group and 63.5 ± 38.4 ng/g in the 0.42 MPa group. However, at 336 h, ADU concentrations in the Sham and 0.25 MPa groups dropped below the detection limit. In contrast, the 0.42 MPa ultrasound-treated group exhibited a tendency for ADU levels to remain detectable up to 336 h (4.0 ± 3.8 ng/g) (Fig. 3A). Plasma ADU levels decreased gradually over time in all groups and were undetectable at 336 h post-administration. The C_{max} in the plasma was 15,006.9 ± 2561.4 ng/mL for the sham control group, 17,554.8 ± 3191.2 ng/mL for the 0.25 MPa group, and 23,933 ± 5038.4 ng/mL for the

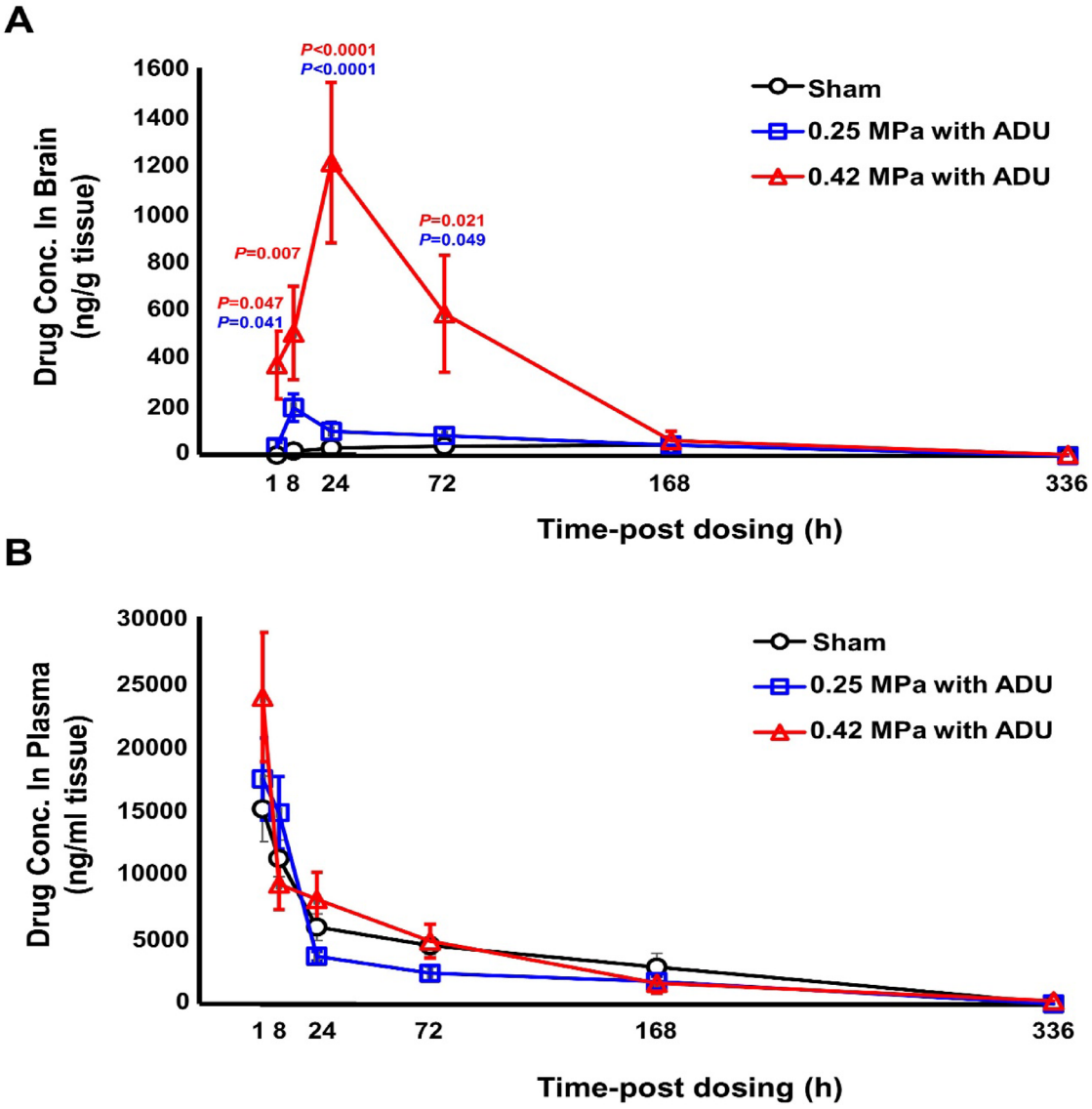

Fig. 3. Time-dependent changes of Aducanumab (ADU) penetrations in the region of focused ultrasound-induced blood-brain barrier disruption (FUS-BBBD). (**A**-**B**) Time-dependent ADU concentrations changes in (**A**) brain and (**B**) plasma after FUS-BBBD with no acoustic pressure (sham), 0.25 MPa, and 0.42 MPa.

0.42 MPa group (Fig. 3B). These findings demonstrate that FUS-BBBD significantly enhances the brain delivery of large-molecule antibody therapeutics by modulating BBB permeability.

ADU distribution in the brain following FUS-BBBD

To further validate ADU delivery to the FUS-BBBD targeted brain regions, we conducted immunohistochemistry using an Alexa Fluor 555-conjugated anti-human IgG antibody to visualize ADU distribution. We selected the 24-hour time point for analysis, as this corresponded to the maximal increase in ADU delivery. Furthermore, the ROI designated for analysis was carefully aligned with the region where BBBD was induced by FUS, ensuring consistency with Fig. 2B and C. Representative images from both FUS pressure conditions and sham controls are shown (Figs. 4A-D). Consistent with the enhanced signal observed in contrast agent-enhanced regions (Figs. 2B-D), ADU was localized to the targeted brain areas, particularly in the thalamus, 24 h post-sonication. The amount of ADU delivered increased with the degree of BBB disruption, showing a 6.9 ± 9.1-fold increase in the 0.25 MPa group and a 63.3 ± 29.2-fold increase in the 0.42 MPa group compared to sham controls (Figs. 4C-E). In the absence of FUS-BBBD, only minimal ADU was detected in the targeted brain regions of the sham control group (Figs. 4B, E).

Safety assessment of FUS-BBBD in vivo

To evaluate potential tissue damage caused by FUS-induced BBBD, we conducted histological analyses using hematoxylin and eosin (H&E) and Nissl staining, as shown in Fig. 5. In the 0.25 MPa group, no evident tissue or cellular damage, such as microhemorrhages, neuronal loss in terms of morphology and density, or tissue cavities, was observed compared to the untreated control and ADU-only sham control groups (Figs. 5A-C, E-G). In contrast, in the 0.42 MPa group, although no significant extravasation of red blood cells (RBCs) indicative of microhemorrhages was detected, small cavities, which may result from excessive ultrasound energy deposition, were observed. Additionally, a significant reduction in neuronal density was observed in the same region, indicating localized neuronal damage (Figs. 5D, H). These findings indicate that while the 0.25 MPa group successfully induced BBBD without histological damage, the 0.42 MPa group caused excessive BBBD accompanied by tissue and cellular damage, consistent with our previous reports[26].

Discussion

In this study, we evaluated the efficiency of ADU delivery enhanced by FUS-BBBD in the normal ICR mouse brain, demonstrating that MRgFUS significantly increased ADU penetration via transient BBB disruption. The amount of ADU delivered was directly correlated with the acoustic pressure amplitude (MPa) of FUS and remained elevated for up to one week post-BBBD. Immunohistochemical analysis evaluated the safety of the procedure. These findings indicate that FUS-BBBD is a promising approach for improving drug delivery to the brain and has potential for clinical applications with further investigation.

We selected two different ultrasound exposure levels (0.25 and 0.42 MPa) based on our previous research on the safety of FUS-induced BBB disruption[26]. The 0.25 MPa condition was chosen because it has been used in preclinical models to achieve effective BBB opening with minimal tissue damage, while the 0.42 MPa condition was selected to evaluate the trade-off between enhanced ADU delivery and potential adverse effects. Although this higher pressure level facilitated greater antibody penetration, mild tissue damage was observed, highlighting the need for careful optimization of FUS parameters for safe and effective drug delivery.

In addition to the differences observed between the 0.25 MPa and 0.42 MPa groups, a distinct pharmacokinetic pattern was evident between the Sham and FUS-treated groups. In the FUS groups, the temporary physical disruption of the BBB allowed ADU to rapidly diffuse into the brain, leading to an early C_{max} formation (8 h at 0.25 MPa and 24 h at 0.42 MPa). However, as the BBB gradually recovered, further ADU entry was restricted, resulting in a rapid decline in brain concentrations. In contrast, in the Sham group, where the BBB remained intact, ADU entry into the brain was highly restricted, likely due to the limited permeability of large-molecule antibodies across the BBB. As a result, ADU accumulation occurred gradually, with C_{max} reached at 168 h, followed by a slow clearance over time. Although receptor-mediated transcytosis has been suggested as a potential transport mechanism for certain antibodies[36], the primary mechanism of ADU transport across an intact BBB remains unclear and is likely to be minimal. These findings suggest that while FUS-BBBD significantly enhances initial drug delivery, the temporal profile of ADU accumulation and elimination is fundamentally different from passive uptake across an intact BBB. Understanding these pharmacokinetic differences is essential for further optimizing FUS-mediated drug delivery strategies, balancing enhanced permeability with safety considerations.

Previous studies have explored the impact of ultrasound on ADU delivery in animal models of Alzheimer's disease (AD). Leinenga et al. found that scanning ultrasound (SUS), which applies energy over a broad anatomical area, enhanced ADU delivery efficiency and reduced amyloid load, leading to improved cognitive function in aged APP23 mice. In that study, SUS resulted in a 5-fold increase in ADU concentration in the cortex 3 days after nine ADU treatments at 5 mg/kg[25]. Kong et al. reported that FUS increased ADU delivery in five familial AD mutation (5xFAD) mice, demonstrating that 24 h post-FUS and ADU treatment (3 mg/kg), ADU levels in the target brain region increased by 8.1-fold[24].

In our study, we demonstrated that FUS-BBBD significantly enhanced ADU delivery at 3 mg/kg, 24 h post-sonication, with a 3.1-fold increase in the 0.25 MPa group (ELISA) and a 6.9-fold increase (IHC). In the 0.42 MPa group, ADU delivery was further enhanced by 37.5-fold (ELISA) and 63.3-fold (IHC) (Figs. 3 and 4). These findings are consistent with previous reports demonstrating that FUS significantly enhances ADU penetration into the brain. While this overall trend aligns with prior studies, the observed differences in fold increases across studies likely result from variations in BBB integrity between experimental animal models and ultrasound parameters. Additionally, the variation in fold increases observed between ELISA and IHC data is likely due to fundamental differences in detection methods. ELISA quantifies the total ADU concentration

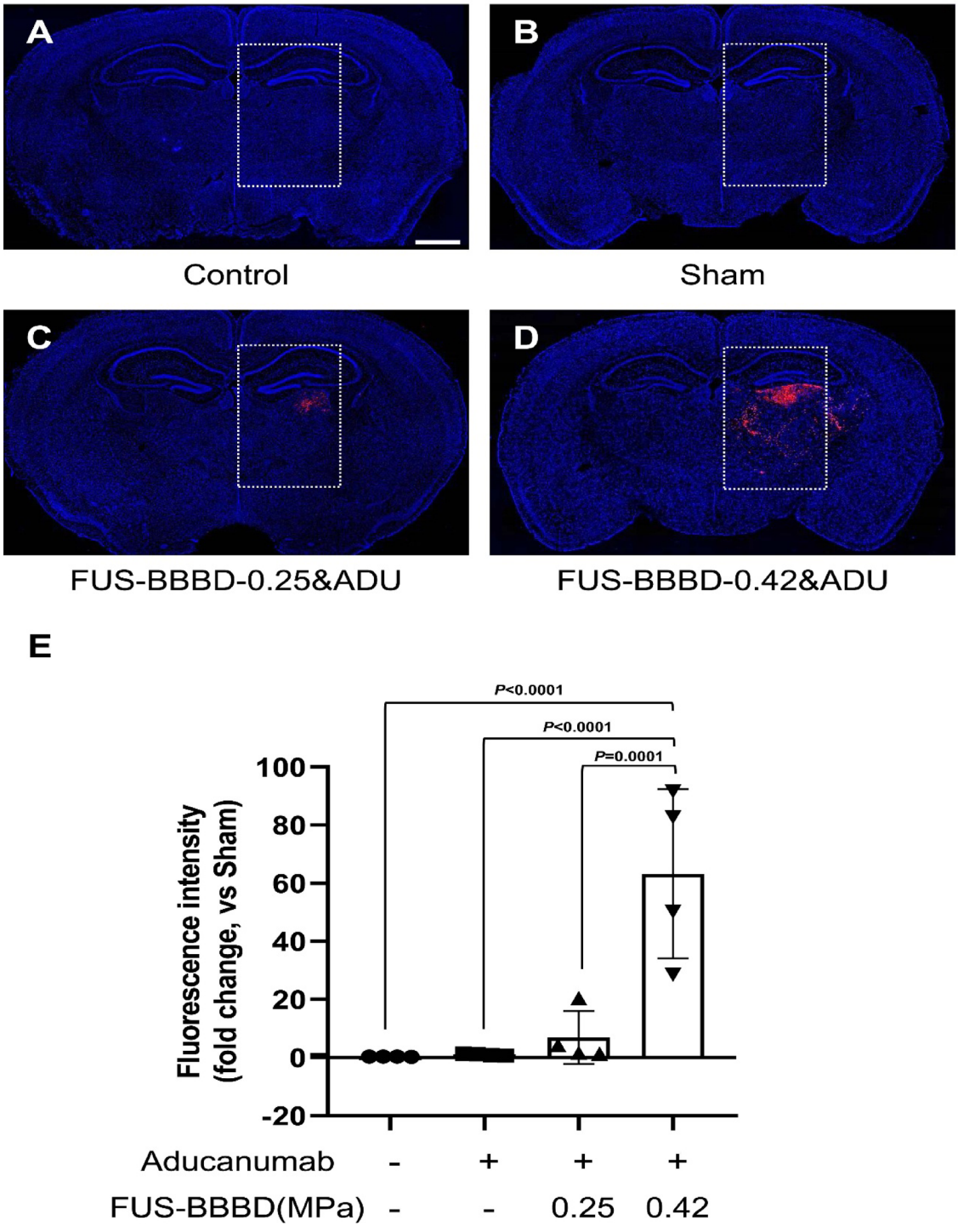

Fig. 4. (**A**-**D**) Immunohistochemical stained brain images for a determination of Aducanumab (ADU) delivery by focused ultrasound-induced blood-brain barrier disruption (FUS-BBBD): (**A**) control, (**B**) sham (FUS-BBBD with no acoustic pressure), (**C**) FUS-BBBD with an acoustic pressure 0.25 MPa, and (**D**) 0.42 MPa. (Blue: DAPI (4′,6-diamidino-2-phenylindole), Red: ADU indicated by Alexa Fluor 555) (**E**) Quantitative data on fold changes in ADU delivery by FUS-BBBD (with an acoustic pressure of 0.25/0.42 MPa) based on sham.

in tissue homogenates, whereas IHC reflects localized ADU distribution within specific regions of interest, potentially leading to greater fold increases in signal intensity.

In Fig. 4, the ROI for ADU signal intensity analysis was selected to align with the BBB opening observed in MRI scans, ensuring consistency across different FUS exposure conditions. The dimensions were standardized based on the broader and more uniform BBB opening in the 0.42 MPa group, allowing for a reliable

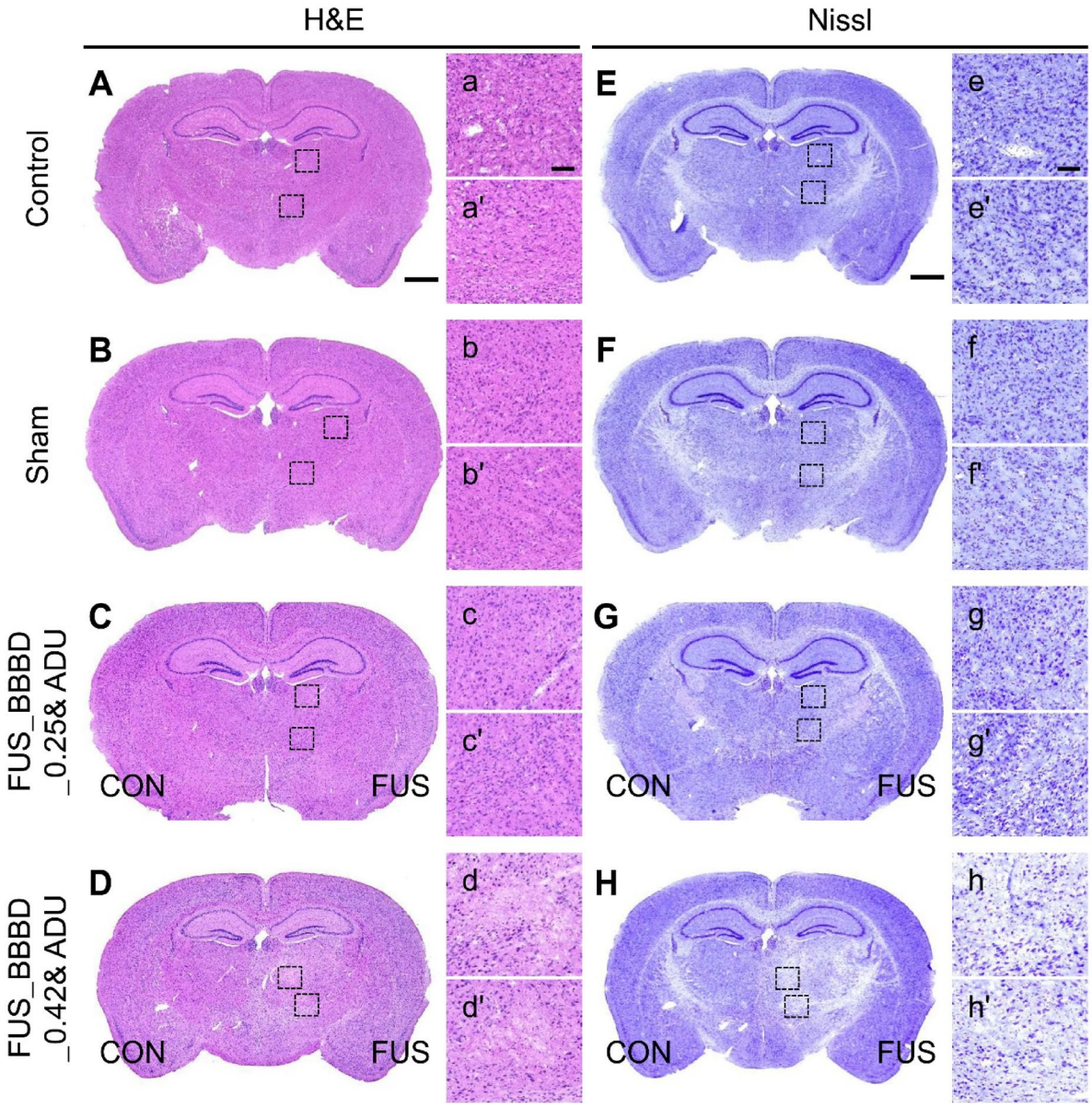

Fig. 5. Safety determination of focused ultrasound-induced blood-brain barrier disruption (FUS-BBBD) using histopathological staining of hematoxylin & eosin (H&E) and Cresyl Violet (Nissl). Histopathological slide scan images of (**A**-**D**) H&E and (**E**-**H**) Nissl-stained brain tissue slides under focused ultrasound conditions: (**A**, **E**) control, (**B**, **F**) sham with no acoustic pressure, (**C**, **G**) FUS-BBBD with an acoustic pressure of 0.25 MPa and (**D**, **H**) 0.42 MPa. The sub-images placed on the right side of each histopathological brain slide image are enlarged images of the rectangular region in the slide image.

comparison of ADU distribution. Despite this, ADU distribution in the 0.42 MPa group exhibited greater spatial heterogeneity, likely due to variations in BBB permeability and enhanced drug dispersion beyond the initial sonicated region. These findings highlight the need to consider both BBB opening extent and subsequent drug penetration dynamics when optimizing FUS-mediated drug delivery. Future studies should explore how different FUS parameters influence BBB permeability and drug diffusion to improve targeted delivery strategies. This variability in ADU distribution may also be influenced by the absence of specific target binding in wild-type mice, where amyloid-beta plaques are not present. In this context, ADU likely undergoes passive diffusion and retention following FUS-mediated BBB opening, rather than binding to a particular target. While non-specific interactions with brain tissue components cannot be ruled out, our study primarily focused on evaluating the efficiency of FUS-enhanced antibody delivery.

Although AD mouse models exhibit a compromised BBB, the extent and heterogeneity of BBB disruption vary significantly depending on disease progression and model characteristics[37,38]. The enhanced ADU delivery observed in wild-type ICR mice compared to AD models may be due to the controlled and uniform BBB opening induced by FUS-BBBD in a physiologically intact BBB, whereas AD models often exhibit regional variability in

BBB integrity, potentially leading to heterogeneous drug distribution. The differential responses between the two models suggest that BBB dysfunction in AD may not uniformly enhance drug penetration but rather introduce additional variability in drug delivery efficiency.

To better understand these differences, further investigations comparing ADU delivery dynamics between AD and wild-type models under identical FUS parameters will be necessary. In particular, future studies using Alzheimer's disease models will help determine how amyloid pathology influences antibody distribution and retention following FUS-BBBD, ultimately guiding the optimization of FUS-mediated drug delivery strategies in disease-relevant conditions.

While MRgFUS is widely regarded as a safe and effective approach compared to other neurosurgical interventions[39–42], a comprehensive evaluation of its potential impact on brain tissue remains essential to ensure its clinical applicability. In this study, we achieved BBB opening without an acoustic monitoring system, relying instead on predefined ultrasound parameters to systematically assess ADU delivery and tissue response. Our previous research demonstrated that BBB opening can be precisely controlled by adjusting acoustic pressure alone, providing a reliable and reproducible method[26]. While real-time acoustic monitoring has been widely used to optimize BBB opening and minimize tissue effects[43], our study was designed to evaluate drug delivery efficiency under controlled exposure conditions. However, we acknowledge that incorporating acoustic feedback control could further enhance treatment monitoring and safety by dynamically adjusting sonication parameters in response to cavitation activity. Future studies will explore this approach to optimize exposure parameters and improve clinical translation.

Our histopathological analysis revealed tissue responses consistent with previous studies. At 0.25 MPa, no detectable tissue damage or neuronal degeneration was observed, while at 0.42 MPa, no extensive pathological abnormalities were detected (Fig. 5). However, small cavities and localized neuronal degeneration were present within the sonicated region. Given the absence of significant erythrocyte extravasation, the observed parenchymal attenuation at 0.42 MPa is more likely attributable to FUS-induced mechanical stress rather than vascular rupture. Nonetheless, the presence of tissue alterations at this pressure level raises concerns regarding potential long-term risks, particularly in patients with AD.

Our previous safety study demonstrated that despite tissue and cellular damage at 0.42 MPa, A2-type astrocytes were activated 48 h post-sonication, suggesting an intrinsic recovery mechanism within the brain microenvironment[26]. However, whether similar recovery pathways are engaged in disease models over extended timeframes remains unknown. Therefore, optimizing FUS parameters to balance drug delivery efficacy and tissue integrity remains a critical challenge. Investigating intermediate pressure conditions between 0.25 and 0.42 MPa or integrating acoustic cavitation monitoring systems[43] may provide valuable insights into enhancing the safety and effectiveness of FUS-BBBD-mediated drug delivery.

Our findings suggest that both the volume of BBB opening and the duration of permeability play a role in ADU delivery, with prolonged BBB opening at higher acoustic pressures being a key factor in enhanced drug accumulation. Specifically, our results demonstrated that while CE-T1W MRI intensity increased 1.8-fold and K_{trans} increased 4-fold, ADU C_{max} increased 6-fold, indicating a non-linear relationship between BBB permeability and drug delivery efficiency. This suggests that the extent of ADU delivery cannot be solely attributed to the volume of BBB opening and that the persistence of BBB permeability may significantly impact drug retention in the brain. Previous studies, including those by Samiotaki and Konofagou et al., have shown that higher acoustic pressures not only increase BBB permeability but also prolong the duration of opening, thereby extending the timeframe for drug diffusion and retention[44]. This aligns with our observation that the 0.42 MPa group exhibited significantly greater ADU accumulation compared to the 0.25 MPa group, despite the difference in BBB opening volume being relatively modest.

Furthermore, the temporal profile of BBB closure varies depending on acoustic pressure, with lower pressures generally leading to rapid recovery, whereas higher pressures result in a prolonged permeability window. If the volume of BBB opening were the sole determinant of drug delivery, a more proportional increase in ADU accumulation would be expected rather than the observed exponential rise at 0.42 MPa. These findings highlight the need for further studies to quantitatively assess the duration of BBB opening under different FUS conditions and to explore strategies for optimizing drug delivery efficiency while minimizing potential tissue effects.

Various strategies, including solid lipid nanoparticles[45], hyperthermia[46], receptor-mediated transcytosis[47], cell-penetrating peptides[48], and cell-mediated drug delivery systems[49], have been explored to enhance drug delivery across the BBB. Despite these efforts, many CNS drug trials have failed due to poor brain penetration[50].

In addition to penetration challenges, many drugs have failed clinical trials. Tarenflurbil (Flurizan, R-flurbiprofen), the R-enantiomer of the non-steroidal anti-inflammatory drugs (NSAID), was used as a gamma-secretase modulator (GSM-I) to lower Aβ 42 levels in preclinical studies[51,52]. However, a phase III study was discontinued owing to poor penetration and ineffectiveness in cognitive decline[53]. The phase I study of Lu AF20513, a vaccine designed to induce humoral response to eliminate Aβ and slow plaque formation, was terminated early due to its poor brain penetration in humans[54,55]. UB-311 is a synthetic peptide vaccine designed to inhibit fibril formation; however, the antibody titers in patients with AD were lower than those previously obtained in a nonhuman primate preclinical study[56]. These examples highlight the ongoing need for improved strategies to enhance CNS drug delivery in clinical trials.

Although Aducanumab has been discontinued, our findings provide valuable insights into FUS-BBBD-mediated antibody delivery, which can be applied to other emerging therapies for AD and neurological disorders. Monoclonal antibodies such as Lecanemab[57] and Donanemab[58] remain under clinical investigation, and the ability to enhance their delivery across the BBB using FUS may improve therapeutic efficacy.

Beyond AD, FUS-BBBD has potential applications in neurodegenerative diseases, brain tumors, and neuroinflammatory conditions, where targeted drug delivery remains a significant challenge. Further research

into FUS optimization, treatment timing, and antibody pharmacokinetics will be essential for translating these findings into clinical applications.

These results underscore the broader relevance of FUS-BBBD as a versatile strategy for enhancing CNS drug delivery, paving the way for future therapeutic advancements.

Conclusions

In this study, we demonstrated that MRgFUS-induced FUS-BBBD temporarily and safely enhances the delivery efficiency of ADU across the BBB. Our findings suggest that FUS-BBBD holds significant potential for advancing drug delivery strategies for intractable brain diseases, such as Alzheimer's disease, by improving therapeutic efficacy while allowing for lower drug dosages. By deepening our understanding of the pharmacokinetics of FUS-BBBD, and extending in vivo preclinical research to large animals, including primates, future clinical studies could establish BBBD via MRgFUS as a transformative approach in the treatment of various neurological disorders. Furthermore, this technique could offer a means to repurpose previously shelved therapeutic agents that were ineffective due to limited BBB penetration, potentially unlocking their full therapeutic potential. Through continued innovation and translational research, FUS-BBBD could redefine treatment paradigms for a wide range of challenging CNS diseases.

Data availability

All data generated or analyzed during this study are included in this published article. The datasets used and/or analyzed during the current study are also available from the corresponding author upon reasonable request. After a permission by publisher, the data presented in this research are available with a presentation of this article as a reference with a statement of information (a title, a journal name, and a publisher).

Received: 16 October 2024; Accepted: 13 May 2025
Published online: 22 May 2025

References

1. Dong, X. Current strategies for brain drug delivery. *Theranostics* **8**, 1481–1493. https://doi.org/10.7150/thno.21254 (2018).
2. Teleanu, R. I. et al. Current strategies to enhance delivery of drugs across the Blood-Brain barrier. *Pharmaceutics* **14** https://doi.org/10.3390/pharmaceutics14050987 (2022).
3. Daneman, R. & Prat, A. The blood-brain barrier. *Cold Spring Harb Perspect. Biol.* **7**, a020412. https://doi.org/10.1101/cshperspect.a020412 (2015).
4. Luissint, A. C., Artus, C., Glacial, F., Ganeshamoorthy, K. & Couraud, P. O. Tight junctions at the blood brain barrier: physiological architecture and disease-associated dysregulation. *Fluids Barriers CNS.* **9**, 23. https://doi.org/10.1186/2045-8118-9-23 (2012).
5. Kadry, H., Noorani, B. & Cucullo, L. A blood-brain barrier overview on structure, function, impairment, and biomarkers of integrity. *Fluids Barriers CNS.* **17**, 69. https://doi.org/10.1186/s12987-020-00230-3 (2020).
6. Banks, W. A. Characteristics of compounds that cross the blood-brain barrier. *BMC Neurol.* **9** (Suppl 1). https://doi.org/10.1186/1471-2377-9-S1-S3 (2009).
7. Han, L. Modulation of the Blood-Brain barrier for drug delivery to brain. *Pharmaceutics* **13** https://doi.org/10.3390/pharmaceutics13122024 (2021).
8. Chen, K. T., Wei, K. C. & Liu, H. L. Theranostic strategy of focused ultrasound induced Blood-Brain barrier opening for CNS disease treatment. *Front. Pharmacol.* **10**, 86. https://doi.org/10.3389/fphar.2019.00086 (2019).
9. Chuang, C. F., Phan, T. N., Fan, C. H., Le, V., Yeh, C. K. & T. T. & Advancements in ultrasound-mediated drug delivery for central nervous system disorders. *Expert Opin. Drug Deliv.* **22**, 15–30. https://doi.org/10.1080/17425247.2024.2438188 (2025).
10. Burgess, A., Shah, K., Hough, O. & Hynynen, K. Focused ultrasound-mediated drug delivery through the blood-brain barrier. *Expert Rev. Neurother.* **15**, 477–491. https://doi.org/10.1586/14737175.2015.1028369 (2015).
11. McDannold, N., Vykhodtseva, N. & Hynynen, K. Effects of acoustic parameters and ultrasound contrast agent dose on focused-ultrasound induced blood-brain barrier disruption. *Ultrasound. Med. Biol.* **34**, 930–937 (2008).
12. Choi, J. J. et al. Noninvasive and localized blood-brain barrier disruption using focused ultrasound can be achieved at short pulse lengths and low pulse repetition frequencies. *J. Cereb. Blood Flow. Metab.* **31**, 725–737. https://doi.org/10.1038/jcbfm.2010.155 (2011).
13. Chopra, R., Vykhodtseva, N. & Hynynen, K. Influence of exposure time and pressure amplitude on blood-brain-barrier opening using transcranial ultrasound exposures. *ACS Chem. Neurosci.* **1**, 391–398. https://doi.org/10.1021/cn9000445 (2010).
14. Vlachos, F., Tung, Y. S. & Konofagou, E. Permeability dependence study of the focused ultrasound-induced blood-brain barrier opening at distinct pressures and microbubble diameters using DCE-MRI. *Magn. Reson. Med.* **66**, 821–830. https://doi.org/10.1002/mrm.22848 (2011).
15. Shin, J. et al. Focused ultrasound-mediated noninvasive blood-brain barrier modulation: preclinical examination of efficacy and safety in various sonication parameters. *Neurosurg. Focus.* **44**, E15. https://doi.org/10.3171/2017.11.FOCUS17627 (2018).
16. Jones, R. M. & Hynynen, K. Advances in acoustic monitoring and control of focused ultrasound-mediated increases in blood-brain barrier permeability. *Br. J. Radiol.* **92**, 20180601. https://doi.org/10.1259/bjr.20180601 (2019).
17. Arndt, J. W. et al. Structural and kinetic basis for the selectivity of aducanumab for aggregated forms of amyloid-beta. *Sci. Rep.* **8**, 6412. https://doi.org/10.1038/s41598-018-24501-0 (2018).
18. Sevigny, J. et al. The antibody aducanumab reduces Abeta plaques in Alzheimer's disease. *Nature* **537**, 50–56. https://doi.org/10.1038/nature19323 (2016).
19. Dunn, B., Stein, P. & Cavazzoni, P. Approval of aducanumab for alzheimer Disease-The FDA's perspective. *JAMA Intern. Med.* **181**, 1276–1278. https://doi.org/10.1001/jamainternmed.2021.4607 (2021).
20. Schneider, L. A resurrection of aducanumab for Alzheimer's disease. *Lancet Neurol.* **19**, 111–112. https://doi.org/10.1016/S1474-4422(19)30480-6 (2020).
21. Tampi, R. R., Forester, B. P. & Agronin, M. Aducanumab: evidence from clinical trial data and controversies. *Drugs Context*. **10** https://doi.org/10.7573/dic.2021-7-3 (2021).
22. Alexander, G. C., Emerson, S. & Kesselheim, A. S. Evaluation of aducanumab for alzheimer disease: scientific evidence and regulatory review involving efficacy, safety, and futility. *JAMA* **325**, 1717–1718. https://doi.org/10.1001/jama.2021.3854 (2021).
23. Knopman, D. S., Jones, D. T. & Greicius, M. D. Failure to demonstrate efficacy of aducanumab: an analysis of the EMERGE and ENGAGE trials as reported by biogen, December 2019. *Alzheimers Dement.* **17**, 696–701. https://doi.org/10.1002/alz.12213 (2021).

24. Kong, C. et al. Enhanced delivery of a low dose of aducanumab via FUS in 5xFAD mice, an AD model. *Transl Neurodegener*. **11**, 57. https://doi.org/10.1186/s40035-022-00333-x (2022).
25. Leinenga, G., Koh, W. K. & Gotz, J. A comparative study of the effects of aducanumab and scanning ultrasound on amyloid plaques and behavior in the APP23 mouse model of alzheimer disease. *Alzheimers Res. Ther.* **13**, 76. https://doi.org/10.1186/s13195-021-00809-4 (2021).
26. Choi, H. J. et al. The new insight into the inflammatory response following focused ultrasound-mediated blood-brain barrier disruption. *Fluids Barriers CNS*. **19**, 103. https://doi.org/10.1186/s12987-022-00402-3 (2022).
27. Choi, H. J. et al. Methylene blue delivery mediated by focused Ultrasound-Induced Blood-Brain barrier disruption reduces neural damage and Amyloid-Beta plaques by AQP-4 upregulation. *Biomedicines* **10** https://doi.org/10.3390/biomedicines10123191 (2022).
28. Han, M., Seo, H., Choi, H., Lee, E. H. & Park, J. Localized modification of water molecule transport after focused Ultrasound-Induced Blood-Brain barrier disruption in rat brain. *Front. Neurosci.* **15**, 685977. https://doi.org/10.3389/fnins.2021.685977 (2021).
29. Jung, B., Huh, H., Lee, E. H., Han, M. & Park, J. An advanced focused ultrasound protocol improves the blood-brain barrier permeability and doxorubicin delivery into the rat brain. *J. Control Release*. **315**, 55–64. https://doi.org/10.1016/j.jconrel.2019.10.044 (2019).
30. McMahon, D., Lassus, A., Gaud, E., Jeannot, V. & Hynynen, K. Microbubble formulation influences inflammatory response to focused ultrasound exposure in the brain. *Sci. Rep.* **10**, 21534. https://doi.org/10.1038/s41598-020-78657-9 (2020).
31. Chu, P. C. et al. Focused Ultrasound-Induced Blood-Brain barrier opening: association with mechanical index and cavitation index analyzed by dynamic Contrast-Enhanced Magnetic-Resonance imaging. *Sci. Rep.* **6**, 33264. https://doi.org/10.1038/srep33264 (2016).
32. Ortuno, J. E. et al. DCE@urLAB: a dynamic contrast-enhanced MRI Pharmacokinetic analysis tool for preclinical data. *BMC Bioinform.* **14**, 316. https://doi.org/10.1186/1471-2105-14-316 (2013).
33. Park, J., Zhang, Y., Vykhodtseva, N., Jolesz, F. A. & McDannold, N. J. The kinetics of blood brain barrier permeability and targeted doxorubicin delivery into brain induced by focused ultrasound. *J. Control Release*. **162**, 134–142. https://doi.org/10.1016/j.jconrel.2012.06.012 (2012).
34. Park, J., Aryal, M., Vykhodtseva, N., Zhang, Y. Z. & McDannold, N. Evaluation of permeability, doxorubicin delivery, and drug retention in a rat brain tumor model after ultrasound-induced blood-tumor barrier disruption. *J. Control Release*. **250**, 77–85. https://doi.org/10.1016/j.jconrel.2016.10.011 (2017).
35. Schneider, C. A., Rasband, W. S. & Eliceiri, K. W. NIH image to imageJ: 25 years of image analysis. *Nat. Methods*. **9**, 671–675 (2012).
36. Sonoda, H. et al. A Blood-Brain-Barrier-Penetrating Anti-human transferrin receptor antibody fusion protein for neuronopathic mucopolysaccharidosis II. Molecular therapy. *J. Am. Soc. Gene Therapy*. **26**, 1366–1374. https://doi.org/10.1016/j.ymthe.2018.02.032 (2018).
37. Liu, Y., Huber, C. C. & Wang, H. Disrupted blood-brain barrier in 5xFAD mouse model of Alzheimer's disease can be mimicked and repaired in vitro with neural stem cell-derived exosomes. *Biochem. Biophys. Res. Commun.* https://doi.org/10.1016/j.bbrc.2020.02.074 (2020).
38. Montagne, A., Zhao, Z. & Zlokovic, B. V. Alzheimer's disease: A matter of blood-brain barrier dysfunction? *J. Exp. Med.* **214**, 3151–3169. https://doi.org/10.1084/jem.20171406 (2017).
39. Elias, W. J. et al. A randomized trial of focused ultrasound thalamotomy for essential tremor. *N Engl. J. Med.* **375**, 730–739. https://doi.org/10.1056/NEJMoa1600159 (2016).
40. Lipsman, N. et al. Blood-brain barrier opening in Alzheimer's disease using MR-guided focused ultrasound. *Nat. Commun.* **9**, 2336. https://doi.org/10.1038/s41467-018-04529-6 (2018).
41. Ravikumar, V. K. et al. Cost-effectiveness of focused ultrasound, radiosurgery, and DBS for essential tremor. *Mov. Disord.* **32**, 1165–1173. https://doi.org/10.1002/mds.26997 (2017).
42. Xu, Y. et al. Safety and efficacy of magnetic resonance imaging-guided focused ultrasound neurosurgery for Parkinson's disease: a systematic review. *Neurosurg. Rev.* **44**, 115–127. https://doi.org/10.1007/s10143-019-01216-y (2021).
43. O'Reilly, M. A. & Hynynen, K. Blood-brain barrier: real-time feedback-controlled focused ultrasound disruption by using an acoustic emissions-based controller. *Radiology* **263**, 96–106. https://doi.org/10.1148/radiol.11111417 (2012).
44. Samiotaki, G. & Konofagou, E. E. Dependence of the reversibility of focused- ultrasound-induced blood-brain barrier opening on pressure and pulse length in vivo. *IEEE Trans. Ultrason. Ferroelectr. Freq. Control*. **60**, 2257–2265. https://doi.org/10.1109/tuffc.2013.6644731 (2013).
45. Bayon-Cordero, L., Alkorta, I. & Arana, L. Application of solid lipid nanoparticles to improve the efficiency of anticancer drugs. *Nanomaterials (Basel)*. **9** https://doi.org/10.3390/nano9030474 (2019).
46. Liu, H. L. et al. Blood-brain barrier disruption with focused ultrasound enhances delivery of chemotherapeutic drugs for glioblastoma treatment. *Radiology* **255**, 415–425. https://doi.org/10.1148/radiol.10090699 (2010).
47. Pulgar, V. M. Transcytosis to cross the blood brain barrier, new advancements and challenges. *Front. Neurosci.* **12**, 1019. https://doi.org/10.3389/fnins.2018.01019 (2018).
48. Zou, L. L., Ma, J. L., Wang, T., Yang, T. B. & Liu, C. B. Cell-penetrating Peptide-mediated therapeutic molecule delivery into the central nervous system. *Curr. Neuropharmacol.* **11**, 197–208. https://doi.org/10.2174/1570159X11311020006 (2013).
49. Ayer, M. et al. T Cell-Mediated transport of polymer nanoparticles across the Blood-Brain barrier. *Adv. Healthc. Mater.* **10**, e2001375. https://doi.org/10.1002/adhm.202001375 (2021).
50. Jeremic, D., Jimenez-Diaz, L. & Navarro-Lopez, J. D. Past, present and future of therapeutic strategies against amyloid-beta peptides in Alzheimer's disease: a systematic review. *Ageing Res. Rev.* **72**, 101496. https://doi.org/10.1016/j.arr.2021.101496 (2021).
51. Eriksen, J. L. et al. NSAIDs and enantiomers of flurbiprofen target gamma-secretase and lower Abeta 42 in vivo. *J. Clin. Invest.* **112**, 440–449. https://doi.org/10.1172/JCI18162 (2003).
52. Kukar, T. L. et al. Substrate-targeting gamma-secretase modulators. *Nature* **453**, 925–929. https://doi.org/10.1038/nature07055 (2008).
53. Green, R. C. et al. Effect of tarenflurbil on cognitive decline and activities of daily living in patients with mild alzheimer disease: a randomized controlled trial. *JAMA* **302**, 2557–2564. https://doi.org/10.1001/jama.2009.1866 (2009).
54. Davtyan, H. et al. Immunogenicity, efficacy, safety, and mechanism of action of epitope vaccine (Lu AF20513) for Alzheimer's disease: Prelude to a clinical trial. *J. Neurosci.* **33**, 4923–4934. https://doi.org/10.1523/JNEUROSCI.4672-12.2013 (2013).
55. Weninger, S. et al. Active immunotherapy and alternative therapeutic modalities for Alzheimer's disease. *Alzheimers Dement. (N Y)*. **6**, e12090. https://doi.org/10.1002/trc2.12090 (2020).
56. Wang, C. Y. et al. UB-311, a novel UBITh((R)) amyloid beta peptide vaccine for mild Alzheimer's disease. *Alzheimers Dement. (N Y)*. **3**, 262–272. https://doi.org/10.1016/j.trci.2017.03.005 (2017).
57. Zhang, Y., Chen, H., Li, R., Sterling, K. & Song, W. Amyloid β-based therapy for Alzheimer's disease: challenges, successes and future. *Signal. Transduct. Target. Therapy*. **8**, 248. https://doi.org/10.1038/s41392-023-01484-7 (2023).
58. Mintun, M. A. et al. Donanemab in early Alzheimer's disease. *N Engl. J. Med.* **384**, 1691–1704. https://doi.org/10.1056/NEJMoa2100708 (2021).

Acknowledgements
This research was supported by a grant of the Korea Dementia Research Project through the Korea Dementia Research Center(KDRC), funded by the Ministry of Health & Welfare and Ministry of Science and ICT, Republic of Korea (grant number : RS-2021-KH112548). Also, this research was supported by a grant of INNOPOLIS Foundation, funded by Ministry of Science and ICT, Republic of Korea (Grant number: RS-2024-00418133) and Korea Institute for Advancement of Technology, funded by Ministry of Trade, Industry and Energy, Republic of Korea (Grant number: RS-2024-00432516). The funders had no role in study design, data collection and analysis, decision to publish, or preparation of the manuscript.

Author contributions
Jaeyeong Jeong: Conceptualization, Methodology, In vivo preclinical experiment, Histopathological sample preparation, Analysis and validation, Writing—original draft preparation, Writing—review and editing. Mun Han: Conceptualization, Methodology, In vivo preclinical experiment, Histopathological sample preparation, Analysis and validation, Writing—original draft preparation, Writing—review and editing. Soyeon Jeon: Methodology, In vivo preclinical experiment, Histopathological sample preparation, Analysis and validation, Writing—review and editing. Yejin Kim: Methodology, In vivo preclinical experiment, Histopathological sample preparation, Analysis and validation, Writing—review and editing. Hyojin Choi: Methodology, In vivo preclinical experiment, Histopathological sample preparation, Analysis and validation, Writing—review and editing. Woohyuk Choi: Methodology, Analysis and validation, Writing—review and editing. Kihyun Kwon: Methodology, Analysis and validation, Writing—review and editing. Jong-ryul Choi: Methodology, Analysis and validation, Writing—review and editing. Eun-Hee Lee: Research Supervising, Conceptualization, Methodology, In vivo preclinical experiment, Histopathological sample preparation, Analysis and validation, Writing—original draft preparation, Writing—review and editing.All authors have read and agreed to the published version of the manuscript.

Declarations

Competing interests
The authors declare no competing interests.

Ethical approval
All experiments were approved by the Animal Experiment Ethics Committee of Daegu–Gyeongbuk Medical Innovation Foundation (IACUC approval number: KMEDI-22012601-00) and all procedures were conducted in accordance with the guideline. Also, the study was carried out in compliance with the ARRIVE (Animal research: reporting of in vivo experiments) guidelines (https://arriveguidelines.org/) and all efforts were made to minimize a number of preclinical animals and their pain. Detailed steps of anesthesia to minimize their pain are described in a section of *Materials and Methods*.

Additional information
Supplementary Information The online version contains supplementary material available at https://doi.org/10.1038/s41598-025-02412-1.

Correspondence and requests for materials should be addressed to J.-r.C. or E.-H.L.